PAPER

Check for updates

Imidosulfonate scorpionate ligands in lanthanide single-molecule magnet design: slow magnetic relaxation and butterfly hysteresis in [ClDy{Ph₂PCH₂S(NtBu)₃}₂]†

Jochen Jung, Christina M. Legendre, [ID] Serhiy Demeshko, Regine Herbst-Irmer [ID] and Dietmar Stalke [ID] *

Single-molecule magnets (SMMs) harbour vast opportunities for potential pioneering applications upon optimization like big data storage and quantum computing. Lanthanides were found to be highly suitable candidates in the design of such molecules, as they intrinsically hold a large unquenched orbital momentum and a strong spin–orbit coupling, warranting a high magnetic anisotropy. An indispensable element in successfully tailoring SMMs is the ligand design. Polyimido sulfur ligands offer a promising choice because the polar S^+-N^--bond facilitates both electronic and geometric adaptability to various f-metals. In particular, the acute N–Ln–N bite angle generates advantageous magnetic properties. The [Ph₂PCH₂S (NtBu)₃]⁻ anion, introduced from [(thf)₃K{Ph₂PCH₂S(NtBu)₃}] (**2**) to a series of complexes [ClLn{Ph₂PCH₂S (NtBu)₃}₂] with Ln = Tb (**3a**), Dy (**3b**), Er (**3c**), Ho (**3d**), and Lu (**3e**), provides tripodal shielding of the metal's hemisphere as well as a side-arm donation of a soft phosphorus atom. For the Tb and Er complexes **3a** and **3d**, slow magnetic relaxation (U_{eff} = 235 and 34.5 cm⁻¹, respectively) was only observed under an applied dc field. The dysprosium congener **3b**, however, is a true SMM with relaxation at zero field (U_{eff} = 66 cm⁻¹) and showing a butterfly hysteresis close to 3.5 K. Upon magnetic dilution with the diamagnetic and isostructural lutetium complex **3e** or application of a magnetic field, the energy barrier to spin reversal is increased to 74 cm⁻¹.

Introduction

The realm of single-molecule magnets (SMMs) has continuously expanded since their discovery in 1993.[1] These molecules can be magnetized and remain so upon the removal of the external magnetic field, however only at helium-level temperatures for the vast majority. Their remarkable magnetic properties, potentially transferable to industry for applications such as high-density data storage and spintronics,[2] are mainly due to the magnetic anisotropy created by the paramagnetic metal centre in a particular crystal field. Lanthanides were found to be highly promising candidates in the design of such molecules as they intrinsically possess a large unquenched orbital momentum and a strong spin–orbit coupling.[3] This

warrants a high magnetic anisotropy, even with only one trivalent lanthanide ion as the sole paramagnetic centre in the SMM. These discoveries spurred the studies of mononuclear, lanthanide containing complexes in recent years.[4,5–7] The design of dysprosocenium sandwich cations with bulky, non-coordinating counter-ions allowed to reach operating temperatures above the liquid nitrogen threshold, narrowing the gap between fundamental research and industrial applications. After these major advances in organometallic chemistry, the development of mononuclear SMMs currently suffers stalling and the scientific community is turning to main group chemistry to look for new ligands enhancing SMM properties. Some studies already indicate the underlying potential in the marriage of molecular magnetism with main group chemistry.[8,9–11] More recently, soft elements were even exploited to strongly couple paramagnetic transition metals with lanthanide ions to build promising heterometallic single-molecule magnets.[12]

Known for several years but not sufficiently promoted in the field of molecular magnetism are the polyimido sulfur ligand species $S(NR)_n^{m-}$ (n = 2, 3, and 4 and m = 0 and 2) that have been studied extensively within our group for several

Georg-August Universität Göttingen, Institut für Anorganische Chemie, Tammannstraße 4, 37077 Göttingen, Germany.
E-mail: dstalke@chemie.uni-goettingen.de

years.[13–28] We published many examples of sulfur-imido ligated s,[13–15] p[16] and d-block[13,17–19] metal complexes and now exploit that ligand versatility in f-element[20] chemistry to give molecular magnets. The S–N ligand class[25] is particularly beneficial in SMM chemistry because it features a sulfur–imido bond with both ionic and covalent character.[15,21] This renders the ligands highly adaptable and responsive to the various requirements of different metals (size, different electronegativity and redox potential, etc.), both geometrically and electronically.

The first results with this ligand class[18,19,22,23] indicated the next steps for synthetic and structural improvements in lanthanide complexes,[20] so far scarcely investigated.[20,24] From the plethora of our SN ligands, we identified the [Ph$_2$PCH$_2$S(NtBu)$_3$]$^-$ scorpionate anion[28] as the most suitable candidate for the following reasons. In addition to three responsive S$^{\delta+}$–N$^{\delta-}$ bonds arranged in a potential cap shaped tripodal fashion, it holds a soft P-donating side-arm. For transition metal SMMs, various examples demonstrate how the introduction of heavier and softer p-block donor atoms improved the magnetic properties.[23] Phosphorus donating ligands in trigonal planar Fe(II)[19,26,27] and Co(II)[19,27] complexes raise the effective energy barriers U_{eff} to undergo a significant spin reversal.[19,23] The enhancement of the zero-field splitting, thanks to the introduction of donor atoms with more diffuse orbitals, was also observed in a series of tetrahedral Co(II) complexes with EPh ligands (E = O, S and Se) that exhibit increasing zero-field splitting descending the group.[9,29,30] Lanthanide-based SMMs with heavier donor atoms are rare and to the best of our knowledge the only example with P-donation improving the magnetic properties is the phospholyl Er(III) complex, in which the Er–P$_{Cp^*}$ interaction, weaker than Er–C$_{Cp^*}$, results in a stronger, more favorable equatorial field.[31] The performance of the bis(phospholyl) Dy(III) cation[11] is not quite on par with either the [Cp*DyCp^{5-iPr}]$^{+5}$ or the [(Cp^{3-tBu})$_2$Dy]$^+$ cation.[6,7] Approaches involving the stacking of magnetically well-performing building blocks[32] or the design of asymmetric complexes modulating the relaxation pathways[33] have proven to be more successful for Er(III) based SMMs. For Dy(III), however, introducing softer atoms is generally considered a good strategy. For example, a series of group 15 bridged dysprosocenes, with the soft donor ligands in the equatorial positions and a strong axial crystal field generated by the cyclopentadienyl ligands, revealed increasing anisotropy barriers from phosphorus to antimony.[10,34,35] These results not only clearly show the necessity to reduce the equatorial crystal field for the development of high-temperature SMMs but also demonstrate the option to improve the molecular magnetism on the basis of softer donor atoms.

For this purpose, we herein propose the [Ph$_2$PCH$_2$S(NtBu)$_3$]$^-$ anion, generated from [(thf)$_3$K{Ph$_2$PCH$_2$S(NtBu)$_3$}] (2), as a potentially suitable candidate for both requests: theoretically an N,N,N- or N,N,P-tripodal ligand, it can shield one hemisphere of the f-metal ion alike Cp-derivatives, and it holds a P-donor side-arm. Thus, we synthesized a series of ligated complexes [ClLn{Ph$_2$PCH$_2$S(NtBu)$_3$}$_2$] with Ln = Tb (3a),

Dy (3b), Er (3c), Ho (3d), and Lu (3e) and analysed their magnetic properties.

Results and discussion

Synthesis and crystallography

Deprotonation of 1 with K(HMDS) in thf gives the potassium complex [(thf)$_3$K{Ph$_2$PCH$_2$S(NtBu)$_3$}] (2) (Scheme 1) that is employed as the ligand source in the subsequent lanthanide transmetallation reactions. Crystallization of 2 in a mixture of n-pentane/thf at −34 °C yielded colourless crystals suitable for X-ray structure analysis. [K(thf)$_3${Ph$_2$PCH$_2$S(NtBu)$_3$}] (2) loses the coordinating thf molecules when stored at room temperature over time and all thf molecules can be removed under reduced pressure (see Fig. S7†). 2 crystallizes in the monoclinic space group $P2_1/n$ with one molecule in the asymmetric unit (Fig. 1). The potassium ion is five-coordinated by only one nitrogen and the phosphorus atom, both from the triimidosulfonate ligand and the additional three thf solvent molecules. In contrast to the other structural motifs of this ligand, it does
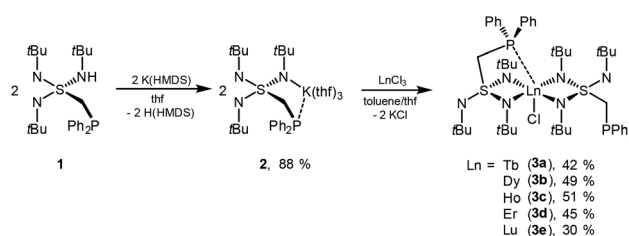
Scheme 1 Synthesis of the potassium starting material [(thf)$_3$K{Ph$_2$PCH$_2$S(NtBu)$_3$}] (2) and the lanthanide complexes [ClLn{Ph$_2$PCH$_2$S(NtBu)$_3$}$_2$] 3a–e (a: Ln = Tb, b: Dy, c: Ho, d: Er, and e: Lu).
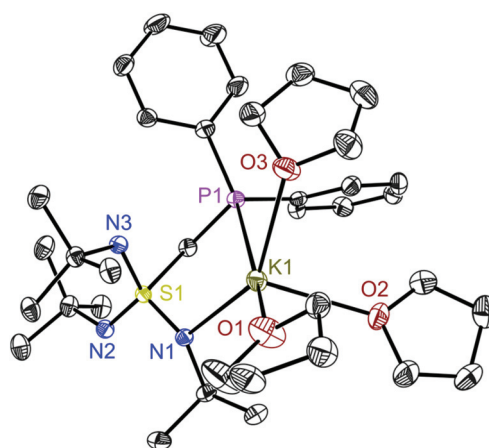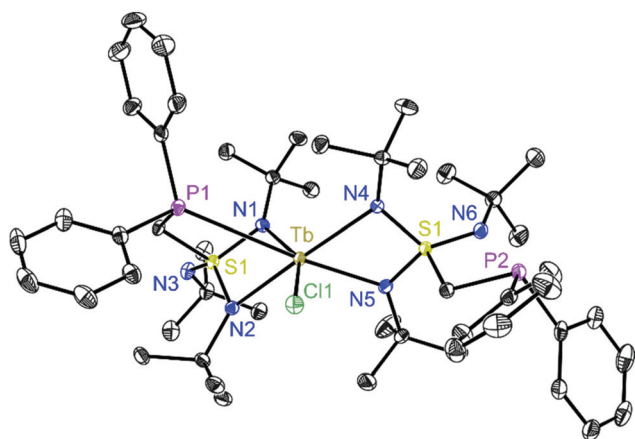

Fig. 1 Crystal structure of [(thf)$_3$K{Ph$_2$PCH$_2$S(NtBu)$_3$}] (2). Anisotropic displacement parameters are depicted at the 50% probability level. Hydrogen atoms and minor positions of the disordered thf molecules are omitted for clarity. Selected bond lengths [Å] and angles [°]: K1–N1 2.7434(14), K1–P1 3.3301(6), N1–S1–N2 109.56(7), N1–S1–N3 110.32(7), N2–S1–N3 122.66(7), N1–S1–C13 108.68(7), N2–S1–C13 108.07(7), N3–S1–C13 96.13(7), N1–K1–P1 69.44(3).

not even function as an N,N′ chelating ligand. The three S1–N bond distances in **2** are similar (av. 1.5578 Å) but due to potassium coordination, the S1–N1 bond (1.5685(14) Å) is the longest. Nevertheless, it is still short compared to the S–N(H) bond distance of 1.6498(13) Å in **1**.[19,28] The coordination of the hard proton has therefore a much more pronounced impact than that of the soft potassium metal. The K1–P1 bond distance of 3.3301(7) Å is in the normal range for a potassium phosphorus bond. In comparison, the P–Li distance of the lithium species [(tmeda)Li{Ph$_2$PCH$_2$S(NtBu)$_3$}][13] is 3.718 Å, too long to be considered a bond (Fig. 2). The K1–N1 bond distance of 2.7434(14) Å falls as well in the normal range covered by a five-fold coordinated potassium ion. The coordination sphere of the potassium atom is completed by three thf solvent molecules with K–O bond lengths from 2.648(5) to 2.7511(14) Å. Through reduced pressure, they can be removed to give a donor-free powder, insoluble in nonpolar hydrocarbons. The addition of small amounts of thf-d$_8$ enables NMR analysis in solution. In ^{1}H NMR, the three NtBu groups are equivalent and resonate at 1.65 ppm. The two methylene protons show a doublet centred at 3.94 ppm ($^2J_{HP}$ = 5.0 Hz) and the phenyl signals can be found in the normal aromatic region. The potassium complex **2** was then used as a precursor for the synthesis of a series of lanthanide complexes [ClLn{Ph$_2$PCH$_2$S(NtBu)$_3$}$_2$] **3a–e**. First attempts with neat thf as the reaction solvent were unsuccessful and the target products could not be isolated. Thus, to trigger KCl precipitation, we selected the more nonpolar solvent toluene. In the synthesis of **3a–e**, thf-free **2** was first suspended in toluene and approximately 2% by volume of thf was added to form the soluble ligand precursor [(thf)$_3$K{Ph$_2$PCH$_2$S(NtBu)$_3$}] (**2**). After the addition of the appropriate lanthanide(III) chloride salt, the reaction mixture was stirred for one day to allow the formation of the soluble complexes [ClLn{Ph$_2$PCH$_2$S(NtBu)$_3$}$_2$] **3a–e** (**a**: Ln = Tb, **b**: Dy, **c**: Ho, **d**: Er, and **e**: Lu). Subsequently, the precipi-

tated KCl was filtered off and all volatiles were removed under reduced pressure. The raw product was then dissolved in thf and layered with n-pentane. After a few days, crystals suitable for X-ray structure analysis were grown at room temperature. **3a–e** are isomorphous and crystallize in the monoclinic space group C2/c with one molecule in the asymmetric unit. Disordered lattice thf and n-pentane are also present (Fig. S2–6†). The central lanthanide(III) ion is six-fold coordinated. One [Ph$_2$PCH$_2$S(NtBu)$_3$]$^-$ anion coordinates N,N,P-tripodal, while the second is only N,N′-chelating with a pendant P-donor side-arm. The remaining coordination site is occupied by a chlorine atom. As anticipated from the decreasing radii, the Ln–Cl1 bond distances decrease from 2.6174(7) Å in **3a** to 2.5467(5) Å in **3e**. All nitrogen atoms are crystallographically independent but the Ln–N distances in all the complexes span over a relatively narrow range of 2.3259(17) Å (Ln–N5) to 2.4085(18) Å (Ln–N2) in **3a** (largest distances) and from 2.2577(11) Å (Ln–N5) to 2.3393(11) Å (Ln–N2) in **3e** (shortest distances in the **3a–e** series). The four metal-coordinated S–N bonds are almost identical, even among the different complexes **3a–e** and average at 1.604 Å. The pendant S1–N3 and S2–N6 bonds, however, are significantly shorter with an average value of 1.515 Å. Although the Ln–P1 distances, decreasing from 3.2291(7) Å in the terbium complex **3a** to 3.1900(5) Å in the lutetium complex **3e**, are at the end of the range covered by other lanthanide–phosphorus bond distances, this has to be judged as an attractive interaction because the second pendant P-donor is idle, similar to [Dy{PPh$_2$S(NtBu)$_2$}$_2$(μ-Cl$_2$)Li(THF)$_2$].[20b] The average N–Ln–N angle of 60.7° is very acute and ranges from 59.7° in **3a** to 62.2° in **3e**. For superior magnetic properties, the linear arrangement of the ligands seems to be advantageous. A key feature in this respect is the S···Ln···S angle. In the series of [Dy{PPh$_2$S (NtBu)$_2$}$_2$(μ-Cl$_2$)Li(THF)$_2$], [Dy{PhS(NtBu)$_2$}$_2$(μ-Cl$_2$)Li-(THF)$_2$] and [Dy{MeS(NtBu)$_3$}$_2$(μ-Cl$_2$)Li (THF)$_2$],[20b] it ranges from 108 to 136°, improving among others U_{eff} at 1000 Oe from 56.8 to 72.4 cm^{-1} in the latter complex, which shows slow relaxation even at zero field (U_{eff} = 59.3 cm^{-1}). Here, the average S···Ln···S angle for **3a–3e** is 142°, even closer to linearity. Attempts to characterize the paramagnetic lanthanide complexes **3a–d** by NMR spectroscopy were not successful, while it confirmed the formation of diamagnetic **3e**. The ^{1}H NMR spectra in C$_6$D$_6$ compared with the protonated ligand [Ph$_2$PCH$_2$S (NtBu)$_2$NHtBu] (**1**) and with the thf free potassium precursor [(thf)$_3$K{Ph$_2$PCH$_2$S(NtBu)$_3$}] (**2**) indeed shows the conversion to [LuCl{Ph$_2$PCH$_2$S(NtBu)$_3$}$_2$] (**3e**) (Fig. S12†). The singlet in **2** at 1.65 ppm splits into two singlets. The smaller one at δ = 1.50 ppm corresponds to the pendant NtBu groups. The larger signal at 1.65 ppm is attributed to the coordinating NtBu groups. The methylene protons in **2** (doublet, 3.94 ppm) are shifted as a multiplet to δ = 4.77–5.06. The ^{31}P NMR spectrum shows only one singlet at −24.59 ppm at room temperature in C$_6$D$_6$, indicating a fast on/off coordination exchange among both phosphorus sites. At −20 °C in d$_8$-toluene, the two sites, starting from −24.64 ppm, could be deconvoluted to give two signals at −23.84 and 27.74 ppm, respectively, at −60 °C

Fig. 2 Crystal structure of **3a–e**. Anisotropic displacement parameters are depicted at the 50% probability level for the Tb complex **3a**. Hydrogen atoms and disordered thf/n-pentane lattice solvent are omitted for clarity. For full bond lengths [Å] and angles [°] of all complexes see the ESI.†

(Fig. S23–25†). The obtained LIFDI mass spectra and elemental analyses for **3a–e** further substantiate the successful syntheses and isolation of bulk material, whose magnetic properties were further investigated.

Magnetic susceptibility measurements

We initially measured the temperature dependency of the product $\chi_M T$ for the complexes **3a–d** (Fig. 3). The obtained high-temperature $\chi_M T$ values for **3a–d** 11.81, 14.09, 13.41 and 10.86 cm^3 mol^{-1} K are very close to the expected values for every single ion (expected 11.82, 14.17, 14.04 and 11.48 cm^3 mol^{-1} K, respectively). The minute differences are attributed to the splitting of the ground state. Upon cooling, for complexes **3a–d**, the $\chi_M T$ value first slowly decreases, indicating the thermal depopulation of the Stark sublevels, and then drastically decreases to reach $\chi_M T$ = 7.46, 8.43, 8.29 and 5.39 cm^3 mol^{-1} K, respectively.

We probed the presence of slow magnetic relaxation with a measurement of the temperature dependence of in-phase (χ'_M) and out-of-phase (χ''_M) ac magnetic susceptibility at 0 Oe and 1000 Oe (see Fig. S26, 30, 39 and 41†). For the Tb (**3a**) and Er (**3d**) complexes, slow magnetic relaxation was only observed under an applied dc field and up to 25 K and 5 K, respectively (see the ESI Fig. S26† for **3a** and S41† for **3d**). The optimal dc field was probed with an additional measurement of the field dependence of the ac magnetic susceptibility at 25 and 5 K, respectively (see Fig. S26 and S41†). The maximal ac magnetic susceptibility values were already reached by 1000 Oe for both Tb and Er complexes. The magnetic relaxation times τ were extracted from the fitting plots of χ''_M *vs.* χ'_M using the CCfit program[36] (Fig. S29 and S43†) and were then used to obtain the temperature dependence plot of the relaxation time (Fig. 4).

These plots indicated the nature of the involved relaxation pathways and the height of the energy barrier associated with the Orbach-type relaxation. The relaxation time τ data measured under 1000 Oe for **3a** and **3d** were fitted according
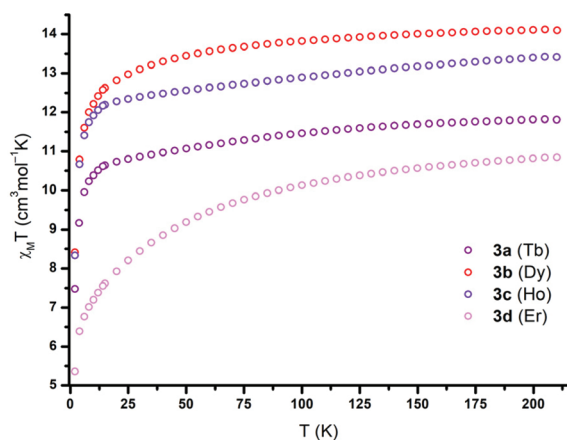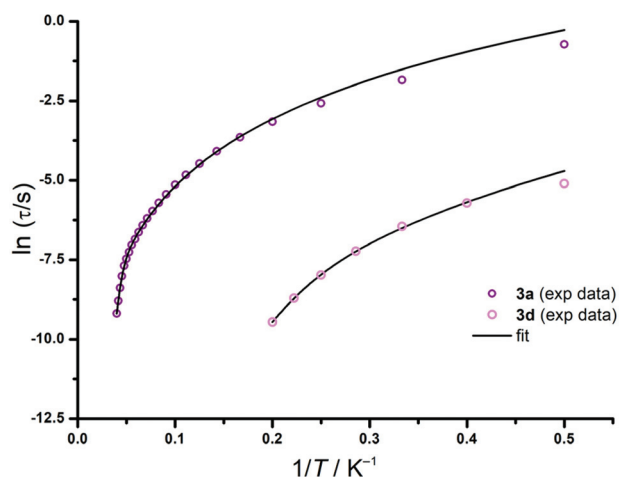

Fig. 4 Temperature dependency plots of the relaxation time plots for complexes **3a** and **3d** under an applied field of 1000 Oe and their corresponding fits (solid black line) according to eqn (1).

to the following equation taking Orbach and Raman processes into account:

$$\tau^{-1} = \tau_0^{-1}\,e^{(U_{eff}/k_B T)} + \tau_{QTM}^{-1} + CT^n \qquad (1)$$

where C and n are the Raman parameters, τ_0 is the initial characteristic relaxation rate for the Orbach process, U_{eff} is the effective energy barrier for spin reversal, k_B is the Boltzmann constant, and τ_{QTM} is the relaxation rate for quantum tunneling of the magnetization (QTM). For **3a**, the observation of a relatively high energy barrier of 235 cm^{-1} (Table 1) is due to the application of an external field, enabling the suppression of quantum tunneling processes at low temperatures. For **3d** (Er), also a field induced SMM, the maxima in the out-of-phase ac magnetic susceptibility was observed up to 5 K under 1000 Oe (Fig. S43†). Similar to **3a**, the fitting of the temperature dependence plot of the relaxation time yielded an effective energy barrier to spin reversal with U_{eff} = 34.5 cm^{-1} and relaxation time τ_0 = 7.3 10^{-9} s (Table 1 and Fig. 4). An applied external dc field is mandatory to observe the slow mag-

Fig. 3 Temperature dependency of $\chi_M T$ for **3a–d** under a dc field of 0.5 T.

Table 1 Fitted parameters of the ac magnetic data for **3a–d** at 0 and 1000 Oe

Complex	3a	3b	3d
H_{dc} (Oe)	1000	1000	1000
U_{eff} (cm^{-1})	235	73.9	34.5
τ_0 (s)	1.9×10^{-9}	2.7×10^{-8}	7.3×10^{-9}
C (s^{-1} K^{-n})	0.17	0.012	5.2
n	3.0	4.2	4.4
Complex	3b	3b@Lu	3b@Lu
H_{dc} (Oe)	0	0	1000
U_{eff} (cm^{-1})	66.5	71.0	74.3
τ_0 (s)	1.2×10^{-7}	2.9×10^{-8}	2.3×10^{-8}
C (s^{-1}K^{-n})	6.5×10^{-2}	1.6×10^{-2}	6.6×10^{-3}
n	4.0	4.4	4.5
τ_{QTM} (s)	1.1×10^{-3}	—	—

netic relaxation of the magnetization for **3a** and **3d**, removing potential QTM. Both complexes can therefore be classified as field induced SMMs.

The holmium analog **3c** does not show slow magnetic relaxation even under an applied dc field as Ho^{3+} ions are non-Kramers ions with a high m_J state mixing rate in the absence of perfectly symmetric ligand fields.[3b] Since dysprosium-containing molecules are more prone to show SMM behaviour, we thus expected even better magnetic properties for the Dy complex **3b**. Remarkably, peaks in the out-of-phase ac dynamic susceptibility were indeed observed for **3b** up to 12 K without any applied dc field, indicative of true SMM behaviour (Fig. S30–32†). At low temperatures, the peaks decrease in intensity without showing any frequency dependence, which strongly suggests the presence of quantum tunneling processes until 5.6 K. The temperature dependence plot of the relaxation time obtained from the fitting of the χ''_M vs. χ'_M Cole–Cole plot reflects the presence of multiple relaxation pathways. A fit according to eqn (1) yields an energy barrier $U_{eff} = 66.5$ cm^{-1} (Table 1, eqn (1) and Fig. S32†). Along with the Orbach relaxation, the slow relaxation of the magnetization mainly happens through a Raman process ($n \approx 4.0$) at higher temperatures and through QTM at lower temperatures. The presence of quantum tunneling typically prevents magnetic blocking. Consequently, **3b** (Dy) shows a butterfly hysteresis even at 2 K. The hysteresis completely closes at 3.5 K (Fig. 5, top).
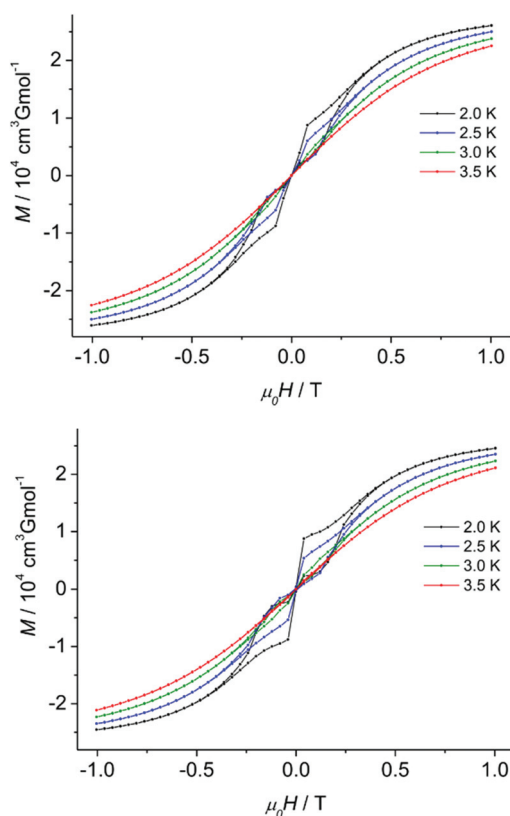
In order to suppress the quantum tunneling effects, we conducted magnetic dilution with the diamagnetic and isostructural lutetium analogue **3e** in a 1 : 10 (Dy : Lu) ratio. Despite the magnetic dilution, the ac magnetic susceptibility measurements of **3b@Lu** still show a temperature independent process until 4.4 K is reached (Fig. S33–35†). However, the out-of-phase signals are shifted to the left and a translation of the peaks to the higher frequencies is noticeable while the temperature is increased (Fig. S33†). Subsequent fitting of the high temperature data gives a thermal energy barrier to spin reversal of U_{eff} = 71.0 cm^{-1} with a relaxation time of $\tau_0 = 2.9\ 10^{-8}$ s (Fig. S35†).

Quite surprisingly, applying an external field on **3b** or on **3b@Lu** shows a similar effect than the magnetic dilution: the maxima for ac dynamic susceptibility were reached at 1000 Oe and data analysis yielded energy barriers of U_{eff} = 73.9 cm^{-1} and 74.3 cm^{-1}, respectively (Table 1, Fig. S38† and Fig. 6). Since the energy barrier values were almost the same for the diluted sample **3b@Lu** and for the pure sample of **3b** at the 1000 Oe dc field, we concluded that further dilution attempts would not improve the energy barrier any further.

Noteworthy, upon magnetic dilution, the shape of the hysteresis obtained for **3b@Lu** slightly improved in comparison with pure **3b**: the wings of the butterfly hysteresis are wider and close at a higher absolute coercive field value (+30 Oe) (Fig. 5, bottom). The wings of the hysteresis, however, completely close at 3.5 K for both the pure and magnetically diluted samples.

Furthermore, we calculated the orientation of the main magnetic axis of the ground state in **3b** (Fig. 7, see section S3.4† for details) based on an electrostatic model.[37] The main magnetic axis is found to be located close to the coordinating nitrogen atoms with the chlorine atom Cl1 perpendicular to it. This suggests that Cl1 contributes to the transverse anisotropy and that the magnetic properties of **3b** could further benefit from its removal. This would probably promote the second phosphorus side arm to coordinate the metal as well as the
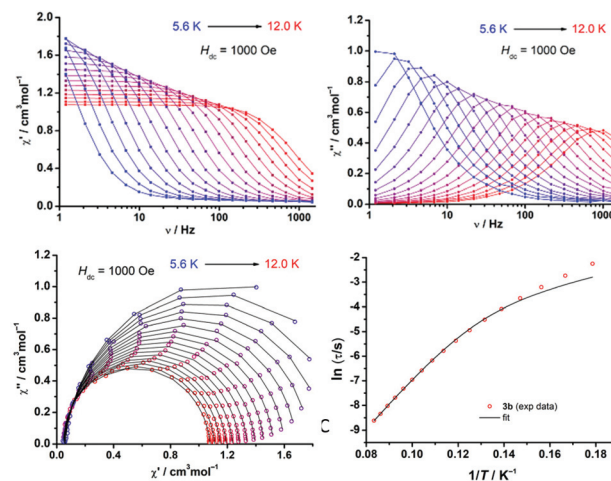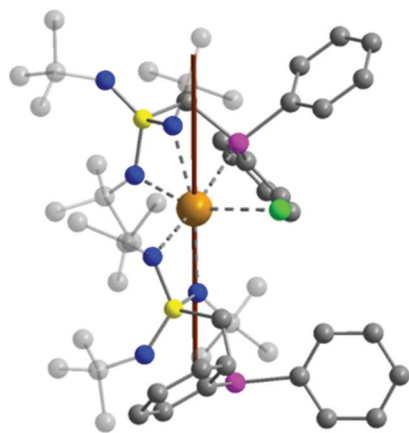

Fig. 5 Magnetic hysteresis for **3b** (top) and **3b@Lu** (bottom) with a sweep rate of 2.7 mT s^{-1}.

Fig. 6 In- and out-of-phase signals of the ac susceptibility at 1000 Oe (top), Cole–Cole plot and Arrhenius plot fitted according to eqn (1) (bottom) for **3b**.

Fig. 7 Orientation of the main magnetic axis of the ground state for the entire molecule of **3b** (brown line). Hydrogens are omitted for better clarity. Orange, green, yellow, pink, dark blue, and grey represent dysprosium, chlorine, sulfur, phosphorus, nitrogen, and carbon atoms, respectively.

linear arrangement of the ligands. Thus, the benefits of the soft donor could be fully assessed and guide further research.

Conclusions

The *N,N,P*-tripodal scorpionate anion $[Ph_2PCH_2S(NtBu)_3]^-$ has emerged to be an ideal ligand in SMMs containing f-metal atoms as paramagnetic centres. The responsive $S^{\delta+}$–$N^{\delta-}$ bonds easily adapt to the electronic and geometric requirements of various metals like terbium to lutetium. Due to their cap-shaped character, they provide a similar steric demand as the omnipresent cyclopentadienide ligands and arrange at an angle of 142°, closer to linearity. This and the acute N–Ln–N angle of 60.7° causes slow magnetic relaxation (U_{eff} = 235 and 34.5 cm^{-1}, respectively) under an applied dc field for the Tb and Er complexes **3a** and **3d**. The dysprosium congener **3b**, however, is an SMM at zero field (U_{eff} = 66 cm^{-1}), showing in addition a butterfly hysteresis closing at 3.5 K. The dynamic magnetic properties are slightly improved upon dilution in the diamagnetic lutetium matrix (**3e**) or application of a dc field (U_{eff} increased to 73.9 cm^{-11}). This study shows that the potassium starting material is more promising than its lithium analogue as it prevents alkaline metal halide co-complexation. The next area of action focuses on the removal of the halide coordinated orthogonally to the main magnetic axis, spoiling the magnetic properties of **3b** and preventing the second Ln–P coordination, as well as the increase of the S···Ln···S angle to approach linearity.

Experimental section

General considerations

All experiments were performed under inert conditions in N_2 or Ar, using Schlenk techniques or in an Ar glovebox. Solvents were dried over sodium or potassium, distilled prior to use and stored over molecular sieves (3 Å). Starting materials were purchased commercially and used without further purification. $(Ph_2PCH_2)S(HNtBu)(NtBu)_2$ was synthesized according to the literature known procedure.[13,19,28] NMR spectra were recorded using a Bruker Avance III HD 500 and referenced to a deuterated solvent signal. LIFDI-MS spectra were recorded using a Jeol AccuTOF spectrometer. Elemental analysis (C, H, N, and S) was performed at the Analytische Labor, Institut für Anorganische Chemie, University of Göttingen.

Single crystals were selected under cooling using an X-Temp2 device.[38] The datasets were collected using an Incoatec Ag Microsource[39] with mirror optics and an APEX II detector with a D8 goniometer. The data were integrated with SAINT.[40] A multi-scan absorption correction was applied using SADABS.[41] The structures were solved by SHELXT[42] and refined on F^2 using SHELXL[43] in the graphical user interface ShelXle.[44]

Magnetic data were recorded with a Quantum-Design MPMS-XL-5 SQUID magnetometer equipped with a 5 T magnet. The crystalline solid sample was crushed, charged into a gel capsule and covered with a few drops of a low viscosity inert oil (perfluoropolyether Fomblin YL VAC 25/6; this oil is liquid above 215 K); the use of oil prevents magnetic torqueing and the loss of solvent molecules. The capsule was placed in a non-magnetic sample holder, which was then inserted in the SQUID magnetometer for measurement. The data were analyzed thanks to the CC-fit[36] and Origin programs (see the ESI† for more details).

Synthesis of $[(thf)_3K\{Ph_2PCH_2S(NtBu)_3\}]$ (2)

A solution of $K\{N(SiMe)_3\}_2$ (1.119 g, 5.610 mmol) in thf (15 mL) was added to a solution of $Ph_2PCH_2S(NtBu)_2NHtBu$ (1) (2.500 g, 5.610 mmol) in thf (10 mL) at ambient temperature. After stirring for 1 d, the solvent was removed under reduced pressure. The residue was dissolved in a mixture of *n*-pentane/ thf (15 mL/3 mL) and filtered. Crystallization started within minutes after storing at −34 °C yielding colourless crystals suitable for X-ray analysis. The product was isolated, washed with *n*-pentane (2 × 2 mL) and dried under reduced pressure. Yield: 2.384 g, 4.928 mmol, (88%); ^{1}H NMR (500.13 MHz, 298 K, C_6D_6): δ [ppm] = 1.65 (s, 27H, 3 NC(CH_3)$_3$), 3.94 (d, $^2J_{HP}$ = 5.0 Hz, 2H, PCH_2), 7.07–7.09 (m, 2H, 2 *p*-Ph-*H*), 7.15–7.18 (m, 4H, 2 *m*-Ph-*H*), 7.84–7.87 (s, 2H, *o*-Ph-*H*); ^{13}C{^{1}H} NMR (125.76 MHz, 298 K, C_6D_6): δ [ppm] = 34.00 (s, NC(CH_3)$_3$), 52.73 (s, NC(CH$_3$)$_3$), 66.11 (d, $^1J_{CP}$ = 21.1 Hz, PCH$_2$), 128.22 (s, *p*-Ph-*C*), 128.37 (d, $^3J_{CP}$ = 6.3 Hz, *m*-Ph-*C*), 133.74 (d, $^2J_{CP}$ = 17.4 Hz, *o*-Ph-*C*), 142.28 (d, $^1J_{CP}$ = 9.4 Hz, *ipso*-Ph-*C*); ^{15}N NMR (50.70 MHz, 298 K, C_6D_6): δ [ppm] = −253.33 (s); ^{31}P{^{1}H} NMR (202.46 MHz, 298 K, C_6D_6): δ [ppm] = −18.14 (s); elemental analysis for $C_{25}H_{39}KN_3PS$ (found (calc.) [%]): C 61.73 (62.07), H 7.84 (8.13), N 8.85 (8.69), S 7.44 (6.63).

General synthesis for $[ClLn\{Ph_2PCH_2S(NtBu)_3\}_2]$ (3a–e)

The donor solvent free potassium precursor $[K\{Ph_2PCH_2 S(NtBu)_3\}]$ (500.0 mg, 1.034 mmol) and LnCl$_3$ (0.517 mmol)

were suspended in toluene (40 mL) and thf (0.8 mL) was added. Subsequently, the mixture was stirred for 1 d at ambient temperature. Precipitated KCl was filtered off and the solvent was removed under reduced pressure. The residue was extracted with thf, filtered and the solvent was removed *in vacuo* again. To receive the target compound as crystalline material, the raw product was dissolved in thf (2.5 mL) and layered with *n*-pentane (12.5 mL). Crystallization started within hours up to several days at ambient temperature yielding crystals that were isolated which were then washed with *n*-pentane (2 × 1 mL).

3a: yield: 240.4 mg, 0.2147 mmol (42%); LIFDI-MS: *m/z*: 1047.3 $[M - Cl]^+$; elemental analysis for $C_{50}H_{78}ClN_6P_2S_2Tb$ $(C_{2.12}H_{4.47}O_{0.38})$ (found (calc.) [%]): C 55.78 (55.91), H 7.37 (7.42), N 7.50 (7.51), S 5.82 (5.73). Colour: pale yellow.

3b: yield: 285.3 mg, 0.2540 mmol (49%); LIFDI-MS: *m/z*: 1052.4 $[M - Cl]^+$; elemental analysis for $C_{50}H_{78}ClN_6P_2S_2Dy$ $(C_{2.25}H_{4.99}O_{0.25})$ (found (calc.) [%]): C 55.80 (55.87), H 7.21 (7.45), N 7.57 (7.48), S 5.92 (5.71). Colour: pale yellow.

3c: yield: 298.6 mg, 0.2653 mmol (51%); LIFDI-MS: *m/z*: 1053.3 $[M - Cl]^+$; elemental analysis for $C_{50}H_{78}ClN_6P_2S_2Ho$ $(C_{2.14}H_{4.56}O_{0.36})$ (found (calc.) [%]): C 54.75 (55.63), H 7.30 (7.39), N 7.36 (7.47), S 5.91 (5.70). Colour: pale orange.

3d: yield: 259.8 mg, 0.2303 mmol (45%); LIFDI-MS: *m/z*: 1056.3 $[M - Cl]^+$; elemental analysis for $C_{50}H_{78}ClN_6P_2S_2Er$ $(C_{2.09}H_{4.38}O_{0.41})$ (found (calc.) [%]): C 54.53 (55.46), H 7.20 (7.36), N 7.33 (7.45), S 5.70 (5.68). Colour: pink.

3e: yield: 175.3 mg, 0.1543 mmol (30%); ^1H NMR (500.13 MHz, 298 K, C_6D_6): δ [ppm] = 1.50 (s, 18H, 2 NC(CH_3)_3), 1.65 (s, 36H, 4 Lu-NC(CH_3)_3), 4.77–5.06 (m, 4H, 2 PCH_2), 6.96–7.13 (m, 12H, *m,p*-Ph-*H*), 7.63 (s, 4H, *o*-Ph-*H*), 7.99 (s,4H, *o*-Ph-*H*); $^{13}C\{^1H\}$ NMR (125.76 MHz, 298 K, C_6D_6): δ [ppm] = 33.42 (s, NC(CH_3)_3), 34.24 (s, Lu-NC(CH_3)_3), 54.24 (s, Lu-NC(CH_3)_3), 55.18 (s, NC(CH_3)_3), 64.79 (s br, PCH_2), 128.69–128.77 (m, *m,m,p*-Ph-*C*), 129.53 (s, *p*-Ph-*C*), 133.03 (d, $^2J_{CP}$ = 16.6 Hz, *o*-Ph-*C*), 135.27 (d, $^2J_{CP}$ = 18.6 Hz, *o*-Ph-*C*), 138.77 (s, *ipso*-Ph-*C*); ^{15}N NMR (50.70 MHz, 298 K, C_6D_6): δ [ppm] = −216.5 (s, Lu-NC(CH_3)_3), −218.7 (s, Lu-NC(CH_3)_3) −255.2 (s, (NC (CH_3)_3)); $^{31}P\{^1H\}$ NMR (202.46 MHz, 298 K, C_6D_6): δ [ppm] = −24.59 (s); $^{31}P\{^1H\}$ NMR (161.98 MHz, 298 K, toluene-d_8): δ [ppm] = −24.64 (s); $^{31}P\{^1H\}$ NMR (161.98 MHz, 213 K, toluene-d_8): δ [ppm] = −23.84 (s), −27.74 (s); LIFDI-MS: *m/z*: 1063.6 [M − Cl]^+; elemental analysis for $C_{50}H_{78}ClN_6P_2S_2Lu(C_{2.27}H_{5.08}O_{0.23})$ (found (calc.) [%]): C 55.03 (55.28), H 7.12 (7.37), N 7.48 (7.40), S 6.12 (5.65). Colour: colourless.

Author contributions

D. St. conceived the project idea and supervised the investigation; J. J. synthesized all compounds and generated and analysed the spectroscopic, diffraction and other experimental data; C. M. L. and S. D. conducted the magnetic measurements and analysed the data; and R. H.-I. supervised the diffraction data refinement. All authors wrote and edited the manuscript with input from everybody in the author list.

Conflicts of interest

There are no conflicts to declare.

Acknowledgements

References

1 R. Sessoli, D. Gatteschi, A. Caneschi and M. A. Novak, *Nature*, 1993, **365**, 141.

2 K. V. Raman, A. M. Kamerbeek, A. Mukherjee, N. Atodiresei, T. K. Sen, P. Lazić, V. Caciuc, R. Michel, D. Stalke, S. K. Mandal, S. Blügel, M. Münzenberg and J. S. Moodera, *Nature*, 2013, **493**, 509.

3 (a) N. Ishikawa, M. Sugita, T. Ishikawa, S.-Y. Koshihara and Y. Kaizu, *J. Am. Chem. Soc.*, 2003, **125**, 8694; (b) J. D. Rinehart and J. R. Long, *Chem. Sci.*, 2011, **2**, 2078.

4 (a) K. R. McClain, C. A. Gould, K. Chakarawet, S. J. Teat, T. J. Groshens, J. R. Long and B. G. Harvey, *Chem. Sci.*, 2018, **9**, 8492; (b) C. A. Gould, K. R. McClain, J. M. Yu, T. J. Groshens, F. Furche, B. G. Harvey and J. R. Long, *J. Am. Chem. Soc.*, 2019, **141**, 12967.

5 F.-S. Guo, B. M. Day, Y.-C. Chen, M.-L. Tong, A. Mansikkamäki and R. A. Layfield, *Science*, 2018, **362**, 1400.

6 C. A. P. Goodwin, F. Ortu, D. Reta, N. F. Chilton and D. P. Mills, *Nature*, 2017, **548**, 439.

7 F.-S. Guo, B. M. Day, Y.-C. Chen, M.-L. Tong, A. Mansikkamäki and R. A. Layfield, *Angew. Chem., Int. Ed.*, 2017, **56**, 11445.

8 (a) F.-S. Guo, A. K. Bar and R. A. Layfield, *Chem. Rev.*, 2019, **119**, 8479; (b) J. P. Durrant, J. Tang, A. Mansikkamäki and R. A. Layfield, *Chem. Commun.*, 2020, **56**, 4708; (c) L. R. Thomas-Hargreaves, M. J. Giansiracusa, M. Gregson, E. Zanda, F. O'Donnell, A. J. Wooles, N. F. Chilton and S. T. Liddle, *Chem. Sci.*, 2021, **12**, 3911.

9 J. M. Zadrozny and J. R. Long, *J. Am. Chem. Soc.*, 2011, **133**, 20732.

10 T. Pugh, V. Vieru, L. F. Chibotaru and R. A. Layfield, *Chem. Sci.*, 2016, **7**, 2128.

11 P. Evans, D. Reta, G. F. S. Whitehead, N. F. Chilton and D. P. Mills, *J. Am. Chem. Soc.*, 2019, **141**, 19935.

12 L. E. Darago, M. D. Boshart, B. D. Nguyen, E. Perlt, J. W. Ziller, W. W. Lukens, F. Furche, W. J. Evans and J. R. Long, *J. Am. Chem. Soc.*, 2021, **143**, 8465.

13 E. Carl and D. Stalke, *Chem. – Eur. J.*, 2014, **20**, 15849.

14 (a) R. Fleischer, S. Freitag, F. Pauer and D. Stalke, *Angew. Chem., Int. Ed. Engl.*, 1996, **35**, 204–206; (b) R. Fleischer, S. Freitag, F. Pauer and D. Stalke, *Angew. Chem., Int. Ed. Engl.*, 1996, **35**, 204.

15 R. Fleischer, B. Walfort, A. Gbureck, P. Scholz, W. Kiefer and D. Stalke, *Chem. – Eur. J.*, 1998, **4**, 2266.

16 (*a*) E. Carl and D. Stalke, *Eur. J. Inorg. Chem.*, 2015, 2052; (*b*) B. Walfort, A. P. Leedham, C. R. Russell and D. Stalke, *Inorg. Chem.*, 2001, **40**, 5668.

17 J. Matussek, R. Herbst-Irmer, I. Objartel and D. Stalke, *Dalton Trans.*, 2014, **43**, 15944.

18 E. Carl, S. Demeshko, F. Meyer and D. Stalke, *Chem. – Eur. J.*, 2015, **21**, 10109.

19 J. Jung, C. M. Legendre, S. Demeshko, R. Herbst-Irmer and D. Stalke, *Inorg. Chem.*, 2021, **60**, 9580.

20 (*a*) J. Jung, F. Benner, R. Herbst-Irmer, S. Demir and D. Stalke, *Chem. – Eur. J.*, 2021, **27**, 12310; (*b*) C. M. Legendre, R. Herbst-Irmer and D. Stalke, *Inorg. Chem.*, 2021, **60**, 13982–13989.

21 (*a*) D. Leusser, B. Walfort and D. Stalke, *Angew. Chem.*, 2002, **114**, 2183, (*Angew. Chem., Int. Ed.*, 2002, **41**, 2079); (*b*) D. Leusser, B. Walfort and D. Stalke, *Angew. Chem., Int. Ed.*, 2002, **41**, 2079; (*c*) D. Leusser, J. Henn, N. Kocher, B. Engels and D. Stalke, *J. Am. Chem. Soc.*, 2004, **126**, 1781; (*d*) J. Henn, D. Ilge, D. Leusser, D. Stalke and B. Engels, *J. Phys. Chem. A*, 2004, **108**, 9442.

22 J. Jung, C. M. Legendre, R. Herbst-Irmer and D. Stalke, *Inorg. Chem.*, 2021, **60**, 967.

23 C. M. Legendre, E. Damgaard-Møller, J. Overgaard and D. Stalke, *Eur. J. Inorg. Chem.*, 2021, 3108–3114.

24 S. V. Klementyeva, N. P. Gritsan, M. M. Khusniyarov, A. Witt, A. A. Dmitriev, E. A. Suturina, N. D. D. Hill, T. L. Roemmele, M. T. Gamer, R. T. Boeré, P. W. Roesky, A. V. Zibarev and S. N. Konchenko, *Chem. – Eur. J.*, 2017, **23**, 1278.

25 T. Chivers and R. S. Laitinen, *Chalcogen-nitrogen chemistry, from fundamentals to applications in biological, physical and material sciences*, World Scientific, 2021.

26 P.-H. Lin, N. C. Smythe, S. I. Gorelsky, S. Maguire, N. J. Henson, I. Korobkov, B. L. Scott, J. C. Gordon, R. T. Baker and M. Murugesu, *J. Am. Chem. Soc.*, 2011, **133**, 15806.

27 A. Eichhöfer, Y. Lan, V. Mereacre, T. Bodenstein and F. Weigend, *Inorg. Chem.*, 2014, **53**, 1962.

28 E. Carl, *Metal Complexes of a New Polyimido Sulfur Phosphanyl Ligand*, PhD Thesis, Göttingen University, 2014; http://hdl.handle.net/11858/00-1735-0000-0022-5DB0-9.

29 J. M. Zadrozny, J. Telser and J. R. Long, *Polyhedron*, 2013, **64**, 209.

30 J. M. Zadrozny and J. R. Long, *J. Am. Chem. Soc.*, 2011, **133**(51), 20732–20734.

31 S.-M. Chen, J. Xiong, Y.-Q. Zhang, Q. Yuan, B.-W. Wang and S. Gao, *Chem. Sci.*, 2018, **9**, 7540.

32 K. L. M. Harriman and M. Murugesu, *Acc. Chem. Res.*, 2016, **49**(6), 1158–1167.

33 M. He, X. Chen, T. Bodenstein, A. Nyvang, S. F. M. Schmidt, Y. Peng, E. Moreno-Pineda, M. Ruben, K. Fink, M. T. Garner, A. K. Powell and P. W. Roesky, *Organometallics*, 2018, **37**(21), 3708–3717.

34 T. Pugh, F. Tuna, L. Ungur, D. Collison, E. J. L. McInnes, L. F. Chibotaru and R. A. Layfield, *Nat. Commun.*, 2015, **6**, 7492.

35 T. Pugh, N. F. Chilton and R. A. Layfield, *Chem. Sci.*, 2017, **8**, 2073.

36 D. Reta and N. F. Chilton, *Phys. Chem. Chem. Phys.*, 2019, **21**, 23567.

37 N. F. Chilton, D. Collison, E. J. L. McInnes, R. E. P. Winpenny and A. Soncini, *Nat. Commun.*, 2013, **4**, 2551.

38 (*a*) T. Kottke and D. Stalke, *J. Appl. Crystallogr.*, 1993, **26**, 615; (*b*) D. Stalke, *Chem. Soc. Rev.*, 1998, **27**, 171.

39 T. Schulz, K. Meindl, D. Leusser, D. Stern, J. Graf, C. Michaelsen, M. Ruf, G. M. Sheldrick and D. Stalke, *J. Appl. Crystallogr.*, 2009, **42**, 885.

40 Bruker AXS Inc., *SAINT*, Madison, 2016.

41 L. Krause, R. Herbst-Irmer, G. M. Sheldrick and D. Stalke, *J. Appl. Crystallogr.*, 2015, **48**, 3.

42 G. M. Sheldrick, *Acta Crystallogr., Sect. A: Found. Adv.*, 2015, **71**, 3.

43 G. M. Sheldrick, *Acta Crystallogr., Sect. C: Struct. Chem.*, 2015, **71**, 3.

44 C. B. Hübschle, G. M. Sheldrick and B. Dittrich, *J. Appl. Crystallogr.*, 2011, **44**, 1281.